

Experimental progress on two-dimensional multiferroics

Yuyang Wang(王羽扬), Dacheng Tian(田大铖), and Lan Chen(陈岚)
Citation: Chin. Phys. B, 2026, 35 (**7**): 077511. DOI: 10.1088/1674-1056/ae53b8
http://cpb.iphy.ac.cn; http://iopscience.iop.org/cpb

What follows is a list of articles you may be interested in

The rise of van der Waals multiferroic heterostructures: Interfacial physics and devices

Yihao Zhao(赵一豪), Hongxu Duan(段虹旭), Tai Min(闵泰), and Tao Li(李桃)
Chin. Phys. B, 2026, 35 (**6**): 067501. DOI: 10.1088/1674-1056/ae3e73

Magnetoelectric topology: The rope weaving in parameter space

Ying Zhou(周颖), Ziwen Wang(王子文), Fan Wang(王凡), Haoshen Ye(叶浩燊), and Shuai Dong(董帅)
Chin. Phys. B, 2026, 35 (**2**): 027501. DOI: 10.1088/1674-1056/ae2c6b

Progress on two-dimensional ferrovalley materials

Ping Li(李平), Bang Liu(刘邦), Shuai Chen(陈帅), Wei-Xi Zhang(张蔚曦), and Zhi-Xin Guo(郭志新)
Chin. Phys. B, 2024, 33 (**1**): 017505. DOI: 10.1088/1674-1056/acf65f

Computational studies on magnetism and ferroelectricity

Ke Xu(徐可), Junsheng Feng(冯俊生), and Hongjun Xiang(向红军)
Chin. Phys. B, 2022, 31 (**9**): 097505. DOI: 10.1088/1674-1056/ac7b1b

Origin of itinerant ferromagnetism in two-dimensional Fe_3GeTe_2

Xi Chen(陈熙), Zheng-Zhe Lin(林正喆), and Li-Rong Cheng(程丽蓉)
Chin. Phys. B, 2021, 30 (**4**): 047502. DOI: 10.1088/1674-1056/abd164

TOPICAL REVIEW — Multiferroicity and multicaloric effects

Experimental progress on two-dimensional multiferroics

Yuyang Wang(王羽扬)[1,2,†], Dacheng Tian(田大铖)[1,2,†], and Lan Chen(陈岚)[1,2,‡]

[1] *Institute of Physics, Chinese Academy of Sciences, Beijing* 100190, *China*
[2] *School of Physical Sciences, University of Chinese Academy of Sciences, Beijing* 100049, *China*

(Received 30 January 2026; revised manuscript received 11 March 2026; accepted manuscript online 18 March 2026)

Two-dimensional (2D) multiferroic materials, characterized by the coexistence of multiple ferroic orders at atomic thicknesses governed by interlayer van der Waals (vdW) interactions, have garnered significant attention due to their exotic physical properties and potential for next-generation information storage, logic, and magnetoelectric spintronic applications, particularly in high-density memory and ultralow-power information processing. This review revisits the fundamental concepts of multiferroicity from symmetry and thermodynamic perspectives, classifies the dominant mechanisms responsible for generating multiferroics and their 2D extensions, and discusses specific material systems ranging from intrinsic to engineered multiferroics. The primary objective of this review is to provide a clear roadmap of the current landscape and offer perspectives on key challenges and opportunities in this rapidly developing field.

Keywords: two-dimensional materials, multiferroics, magnetoelectric coupling

PACS: 75.85.+t, 77.55.Nv, 77.80.–e, 75.70.Cn

DOI: 10.1088/1674-1056/ae53b8 **CSTR:** 32038.14.CPB.ae53b8

1. Introduction

Multiferroic materials hosting coupled magnetic, electric, or structural orders have long been explored as a route to electric-field control of magnetism and ultralow-power information processing.[1,2] Classical bulk multiferroics such as $BiFeO_3$[3–5] and rare-earth manganites[6–8] have established the key microscopic mechanisms and symmetry principles behind magnetoelectric coupling. At the same time, they also revealed intrinsic limitations: the chemical and electronic requirements for stabilizing ferroelectricity often conflict with those needed for magnetism,[9] resulting in restricted material choices, relatively weak coupling strengths, and modest transition temperatures. These constraints have motivated sustained efforts to identify new material platforms where ferroic orders could be stabilized and coupled through alternative mechanisms.

The advent of two-dimensional (2D) materials provides precisely such a platform. Since the isolation of graphene[10] and subsequent expansion of van der Waals (vdW) crystals,[11] atomically thin layers have been shown to retain robust lattice, electronic, and magnetic properties while offering unparalleled control over symmetry, stacking, and interlayer registry. In the 2D limit, ferroic orders are not merely reduced-dimensional analogues of bulk phases: reduced dimensionality introduces enhanced fluctuations, modified exchange interactions, and new pathways for inversion and time-reversal symmetry breaking, enabling ferroic behaviors difficult or impossible to realize in three-dimensional solids.

Breakthroughs in 2D ferromagnetism and ferroelectricity independently demonstrated that both order parameters can remain robust and switchable at atomic thickness. Monolayer CrI_3[12] and $Cr_2Ge_2Te_6$[13] verified that long-range magnetic order can survive in 2D when supported by sufficient anisotropy, while materials such as α-In_2Se_3[14] and $CuInP_2S_6$[15] established intrinsic out-of-plane ferroelectricity down to the monolayer limit. Interlayer-sliding ferroelectricity, discovered in WTe_2[16,17] and hBN,[18,19] further revealed that 2D systems can host new polarization mechanisms rooted in stacking geometry rather than classic lattice instabilities. Together, these advances suggest that if magnetism and polarization can be stabilized independently in 2D, their coexistence and coupling i.e., 2D multiferroicity, become a natural and conceptually compelling possibility.[20,21]

Two complementary pathways have since emerged. Intrinsic single-phase 2D multiferroics naturally support simultaneous magnetic and polar orders, while engineered multiferroics exploit interlayer coupling, intercalation, doping, or moiré superlattices to generate emergent magnetoelectric behavior. Beyond ferromagnetic and ferroelectric phases, 2D materials may also host other orders such as ferroelastic and ferrovalley states. Furthermore, this landscape is enriched by functional domain walls and ultrafast nonequilibrium responses.

Taken together, these advances highlight the rapid evolution of 2D multiferroics from a conceptual extension of bulk

[†] These authors contributed equally to this work.
[‡] Corresponding author. E-mail: lchen@iphy.ac.cn
© 2026 Chinese Physical Society and IOP Publishing Ltd. All rights, including for text and data mining, AI training, and similar technologies, are reserved.

multiferroicity into a distinct class of low-dimensional systems with diverse and tunable properties. In this review, we begin by introducing the foundational concepts of ferroic and multiferroic orders. We then delve into the underlying mechanisms of magnetoelectric coupling in 2D systems, followed by a comprehensive survey of representative material realizations, encompassing both intrinsic and engineered 2D multiferroics. Furthermore, we explore expanding frontiers including exotic orders, domain walls, and non-equilibrium dynamics. Finally, we highlight the prevailing challenges and open questions that define the future landscape of this field.

2. From symmetry breaking to Landau theory

Phase transitions and ordering phenomena in condensed matter physics fundamentally originate from the spontaneous breaking of system symmetries. Understanding the evolution from this microscopic mechanism to macroscopic order serves as the theoretical cornerstone for exploring 2D multiferroic materials. This section establishes a framework bridging fundamental symmetry analysis to macroscopic thermodynamic descriptions. We begin with the concept of spontaneous symmetry breaking (SSB) to elucidate the emergence and physical significance of order parameters. Subsequently, we define "ferroic orders" characterized by their switchability and discuss their dynamic behavior under conjugate fields. Building on this, we focus on the classification of multiferroicity (type-I and type-II) based on the Ginzburg–Landau phenomenological theory, which provides a universal theoretical language for the specific discussions of 2D multiferroic materials in subsequent sections.

2.1. Ferroic orders

Here we briefly summarize these well-established concepts to provide a unified language for discussing 2D multiferroics. When a system's Hamiltonian remains invariant under a certain symmetry transformation, yet its ground state fails to preserve this symmetry, which means the symmetry group G becomes a subgroup H, the system is said to undergo SSB. In the thermodynamic limit, the expectation value of a local operator can be defined as an order parameter to characterize the extent of this symmetry breaking.[22] When the system undergoes a phase transition from a high-temperature disordered phase to a low-temperature ordered phase at the critical temperature, the order parameter changes from zero to nonzero:

$$G \to H, \quad \lim_{h\to 0}\lim_{V\to\infty} \left\langle \hat{O} \right\rangle_{h,V} \neq 0. \tag{1}$$

In the above equation, h represents the conjugate field and V is the volume; $\hat{O}$ is the order parameter. SSB splits the initially unique ground state into multiple degenerate configurations, with different degenerate states corresponding to distinct values of the order parameter. However, the presence of defects and thermal or quantum fluctuations prevents perfectly uniform symmetry breaking, leading to the formation of domains in which the order parameter locally selects different degenerate states.[23] Crucially, this degeneracy can be lifted by a conjugate field, which couples to the order parameter and renders one state energetically favorable over others, allowing transitions between different minima in the energy landscape. Such field-driven transitions are typically accompanied by hysteresis, reflecting the existence of finite energy barriers and dissipative processes during domain nucleation and evolution.

A ferroic order is defined by the existence of a spontaneous order parameter in zero external field and by the ability of an external conjugate field to switch between degenerate states, typically accompanied by domain formation and hysteresis.[24] Thermodynamically, one ferroic order may induce another, giving rise to two distinct categories: the spontaneously broken ferroic order is referred to as the primary ferroic order, and the induced ferroic order is referred to as the secondary ferroic order.[25,26] Representative ferroic orders include ferromagnetism, ferroelectricity, and ferroelasticity, which respectively break time-reversal symmetry, spatial inversion symmetry, and specific point-group symmetries. Their corresponding order parameters are the magnetization, polarization, and strain tensors, with magnetic field, electric field, and stress serving as the conjugate fields.

2.2. Multiferroicity

If a phase simultaneously exhibits two or more ferroic orders, it is termed multiferroic.[27] Initially, this term specifically required the presence of two or more primary ferroic orders. However, the scope has since expanded to encompass secondary ferroic orders, with magnetically induced ferroelectricity being a prominent example. According to Khomskii, systems where ferroic orders originate independently are classified as type-I multiferroics, while those in which magnetism causes ferroelectricity and thus strong coupling are termed type-II multiferroics.[28] Once coupling arises between ferroic orders in a multiferroic material, the conjugate field of one ferroic order can modulate another, revealing immense application potential — particularly in the electric-field control of magnetic order. In practice, type-I multiferroics typically exhibit stronger polarization and higher critical temperatures but weaker coupling, whereas type-II multiferroics show the opposite characteristics: stronger coupling, weaker polarization, and lower critical temperatures. A key challenge is to find strongly coupled multiferroics at high temperature, particularly above room temperature.

From a macroscopic thermodynamic perspective, ferroic orders and related coupling phenomena (such as magnetoelectric coupling) can be described using the phenomenological

Ginzburg–Landau framework:[22,29]

$$f(\boldsymbol{P},\boldsymbol{M};T) = f_0(T)+a_P(T)\boldsymbol{P}^2+b_P(T)\boldsymbol{P}^4 +a_M(T)\boldsymbol{M}^2+b_M(T)\boldsymbol{M}^4+\cdots -\boldsymbol{P}\boldsymbol{E}-\boldsymbol{M}\boldsymbol{H}+f_{\rm me}, \quad (2)$$

$$f_{\rm me} = \alpha_{ij}P_iM_j+\beta_{ijkl}P_iP_jM_kM_l+\gamma_{ijk}P_iM_jM_k +\lambda\boldsymbol{P}\cdot(\boldsymbol{M}\times(\nabla\times\boldsymbol{M}))+\cdots. \quad (3)$$

In the above formula, f_0 denotes the baseline free energy of the system when the order parameters are zero, a_P, b_P, and a_M, b_M represent the phenomenological Landau expansion coefficients for polarization P and magnetization M, respectively. $f_{\rm me}$ represents the magnetoelectric coupling, typically including the bilinear term, fourth-order terms, third-order mixed terms, and gradient-related terms.[30] To determine the configuration of the order parameter that minimizes the free energy at a given temperature, partial derivatives are taken with respect to the given order parameter. In the absence of an external field, since the coefficient $a(T)$ changes sign on either side of the critical temperature, the free energy minimum shifts from a zero order parameter to a non-zero order parameter, reflecting SSB, as Fig. 1(a) shows. When an external field is applied, it acts as a constant which shifts the partial derivative and its zero points. As a result, a nonzero order parameter can emerge above the critical temperature, whose value can be modulated by the external field, as Fig. 1(b) shows. Considering the energy barrier between the degenerate states, we can obtain the hysteresis loop as shown in Fig. 1(c). Considering multiple orders and their coupling terms, if ferromagnetism and ferroelectricity emerge independently at their respective critical temperatures, meaning they have separate driving mechanisms, it corresponds to type-I multiferroics. In this case, the coupling terms can alter their critical temperature, the extent of which depends on the order and strength of the coupling terms. If a primary spontaneous order induces a secondary, improper order that would otherwise remain latent through the coupling terms, type-II multiferroics occur. This induction is driven by specific symmetry-breaking coupling, making the secondary order a direct thermodynamic consequence of the primary phase transition.

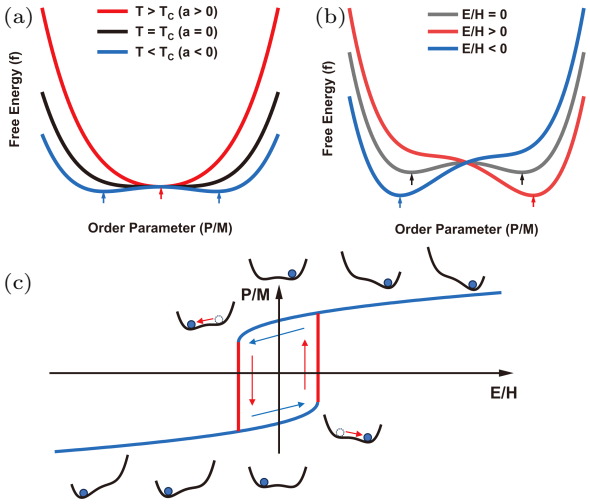


Fig. 1. Symmetry and thermodynamics of ferroics. (a) Evolution of the Landau free energy functional as a function of temperature, illustrating the phase transition from a high-symmetry state ($T > T_c$) to a broken-symmetry state ($T < T_c$). (b) Evolution of the Landau free energy functional as a function of external field $\boldsymbol{E}/\boldsymbol{H}$. (c) Schematic of a hysteresis loop mapped onto the tilting of the double-well potential landscape under an external field $\boldsymbol{E}/\boldsymbol{H}$.

3. Magnetoelectric coupling mechanisms at the 2D limit

In addition to the symmetry and thermodynamic perspectives discussed above, it is essential to incorporate microscopic mechanisms to gain a deeper understanding of multiferroics. From a microscopic perspective, multiferroicity originates from the intricate interplay among spin, charge, orbital, and lattice degrees of freedom. Researchers initially discovered that in classical perovskite oxide multiferroics like $BiFeO_3$, magnetism requires partially occupied d orbitals (d^n), while ferroelectricity demands fully vacant d orbitals (d^0). This contradiction has resulted in a scarcity of multiferroic materials.[9] However, with the advancement of theory and the discovery of new systems, numerous approaches have been developed to circumvent this contradiction.[31] This section begins by delineating the magnetic and ferroelectric mechanisms separately and then moves to their coupling, especially these strong magnetoelectric coupling pathways in type-II multiferroics. Building on this, the focus shifts to the 2D limit, where we introduce the novel interlayer degree of freedom along with the unique stability constraints of the Mermin–Wagner theorem and depolarization fields.

3.1. Magnetoelectric coupling

Magnetism arises from either localized magnetic moments or itinerant electron spin polarization. The multi-orbital Hubbard model is commonly used to describe magnetism. When electrons are highly localized (strongly correlated limit), it can be simplified via second-order perturbation theory into a low-energy effective spin model, namely, the generalized Heisenberg model.[32,33] Even for itinerant electrons, the generalized Heisenberg model is also effective. The bilinear term in its spin Hamiltonian is

$$H_{ij} = -\boldsymbol{S}_i^{\rm T}P_{ij}\boldsymbol{S}_j = -J_{ij}\boldsymbol{S}_i\cdot\boldsymbol{S}_j+D_{ij}\cdot(\boldsymbol{S}_i\times\boldsymbol{S}_j) -\sum_{\alpha\beta}\Gamma_{ij}^{\alpha\beta}S_i^{\alpha}S_j^{\beta}. \quad (4)$$

The first term represents isotropic symmetric exchange (Heisenberg exchange), whose coefficient is a scalar. When the sign is reversed, it favors spin-parallel or spin-antiparallel

alignment, corresponding to ferromagnetic or antiferromagnetic (ferrimagnetic) behavior. This constitutes the most common and prominent contribution to magnetism. The second term is the antisymmetric Dzyaloshinskii–Moriya interaction (DM interaction), whose coefficient is a pseudovector. It originates from spin–orbit coupling (SOC) incorporating relativistic effects and tends to form chiral spin structures such as helical magnetic order and skyrmions.[34,35] The third term is the anisotropic exchange interaction, whose coefficient is a second-order tensor arising from second-order SOC. Higher-order terms, omitted here, can sometimes exert significant effects. In common magnetic materials, the local magnetic moments are primarily contributed by partially filled transition metal 3d orbitals (e.g., Cr, Mn) and rare-earth metal 4f orbitals (e.g., lanthanide elements like Nd, Sm, Dy).

Ferroelectric polarization in solids can be decomposed into contributions from both ions and electrons. The ionic contribution arises from lattice displacement, while the electronic contribution can be described by the Berry phase of the electron wavefunction.[36] Based on the aforementioned Landau theory, ferroelectricity can be categorized into proper types, where polarization is the primary order parameter (spontaneous polarization occurs when the coefficient a changes sign, including displacement/soft-mode and ordered–disordered types), and improper types induced by coupling terms.[37,38] Common non-spin-driven ferroelectric mechanisms include lone pair effects (hybridization between central ions and coordinating anions driving cation displacement from the geometric center, e.g., $BiFeO_3$[39]), d mechanism (hybridization between vacant d orbitals and coordinating atoms softens polar phonon modes, e.g., $BaTiO_3$[40]), geometry-induced (multiple nonpolar modes induce polarization via trilinear terms, e.g., hexagonal $YMnO_3$[8]), and charge ordering (asymmetric charge distribution introduced by different valence states, accompanied by lattice relaxation, e.g., $LuFe_2O_4$,[41] though controversial). Electronic effects often serve as triggers, while lattice responses complete inversion symmetry breaking to stabilize polarization.

The magnetoelectric coupling mechanisms that connect these ferroic orders are equally rich. For instance, in $BiFeO_3$, Bi^{3+} at site A contributes ferroelectricity via its lone pair, while Fe^{3+} at site B contributes collinear antiferromagnetism via its 3d electrons. Since type-I multiferroics exhibit weak magnetoelectric coupling, our primary interest lies in type-II multiferroics, where magnetic order is intrinsically required to break inversion symmetry and induce ferroelectricity, thereby guaranteeing strong coupling.[42] Fundamentally, such intrinsic spin–polarization entanglement in type-II multiferroics not only yields strong linear coupling but also opens the door to topologically protected magnetoelectric responses.[43] Typical examples in three-dimensional multiferroics include: (1) Inverse DM effect/KNB model (Fig. 2(a)): In the DM effect, the pseudovector coefficient depends on the lattice. When SOC is present, the inverse DM effect induces lattice distortion via antiferromagnetic magnetic order, corresponding to the gradient term in the aforementioned Landau theory. An example is $TbMnO_3$ with its helical spin order. The Katsura–Nagaosa–Balatsky (KNB) model (spin current model) offers an alternative interpretation. Formally equivalent to the DM interaction, it describes purely electronic effects under fixed ions, where noncollinear magnetic order induced by SOC contributes to polarization.[44] (2) p–d hybridization (Fig. 2(b)): Due to the anisotropy of SOC, transition amplitudes are larger for identical spin states. Spin states modulate the p–d hybridization between the central atom and coordinating atoms, forming asymmetric electron cloud distributions (local electron density rearrangement), as seen in $CuFeO_2$.[45] (3) Exchange striction (Fig. 2(c)): The scalar coefficient in the symmetric exchange term depends on the relative positions of the two magnetic moments (collinear spin order). Ion displacement alters the equilibrium position, tending to increase the exchange energy and manifesting as exchange striction, as seen in rhombic $RMnO_3$.[46] While the above theories have successfully explained mechanisms in specific materials, they may not always provide satisfactory explanations when applied to other systems and may sometimes coexist.

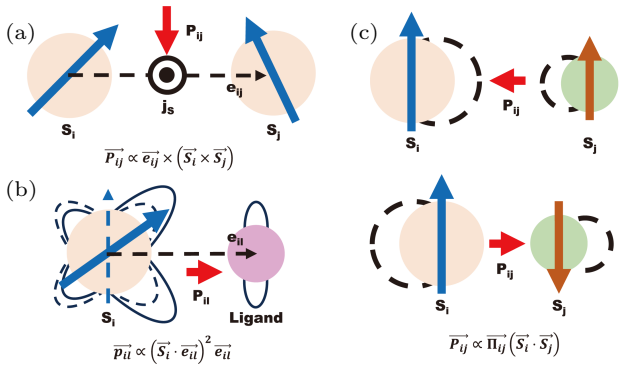


Fig. 2. Schematic illustrations of typical spin-driven magnetoelectric coupling mechanisms in multiferroic materials. (a) KNB model: The spin current model illustrates how noncollinear spin order between metal ions breaks inversion symmetry via spin–orbit coupling to induce polarization. (b) p–d hybridization: Driven by the anisotropy of spin–orbit coupling, where spin states modulate the p–d hybridization efficiency between metal ions and ligands, resulting in an asymmetric local electron density distribution. (c) Exchange striction: collinear magnetic order induces ion displacements through symmetric exchange interactions, thereby breaking inversion symmetry to generate ferroelectricity.

3.2. The 2D characteristics

Beyond canonical pathways in three-dimensional systems, 2D systems introduce novel coupling channels. When dimensions are reduced to the atomic scale, quantum confinement effects discretize the quantum states and restrict the spatial motion of charge carriers, which fundamentally alters the electronic structure compared to bulk counterparts. When combined with pronounced surface effects — such as surface

reconstruction, specific electronic states, adsorption, and passivation — these factors engender physical properties absent in three-dimensional materials.

The 2D materials can be categorized into vdW materials and non-vdW materials (which include both non-vdW layered materials and intrinsically non-layered bulk materials) based on their interlayer bonding mechanisms. Non-vdW materials such as silicene rely on epitaxial growth and exhibit strong coupling with the substrate, necessitating stringent lattice matching requirements and making substrate control critical. In contrast, 2D vdW materials such as graphene are held together by vdW forces between layers. They can be stably obtained through mechanical exfoliation and possess natural cleavage planes. Even epitaxially grown vdW materials lack dangling bonds on their surfaces, exhibit weak interactions with substrates, and are easily separable and transferable, facilitating the realization of hetero-composites. More importantly, distinct interlayer stacking configurations and relative rotations may generate unique properties not observed in single-layer 2D materials (e.g., moiré superlattices, flat bands, and superconductivity[47–49]). This inherent interlayer freedom endows 2D vdW materials with immense potential in multiferroic applications, revealing novel mechanisms such as interlayer sliding ferroelectricity.

In 2D systems, the mechanism of three-dimensional multiferroics also applies. Despite their unique electronic structure, surface states, van der Waals surfaces, and interlayer freedom, there are certain constraints unique to 2D multiferroics.

(1) Thermal fluctuation. The Mermin–Wagner theorem, proven using the Bogoliubov inequality, establishes that in one- and two-dimensional isotropic Heisenberg models with finite-range interactions, spontaneous magnetization or sublattice magnetization cannot exist at finite temperatures; that is, continuous symmetries cannot spontaneously break in thermal equilibrium systems in two dimensions or below.[50,51] This thermal instability stems from the infrared divergence of long-wavelength Goldstone modes inherent in the spontaneous breaking of continuous symmetries. Consequently, the establishment of long-range order necessitates the introduction of anisotropy to open an energy gap. This gap suppresses the divergence of low-energy excitations and effectively shifts the system's symmetry from continuous to discrete, thereby stabilizing the ordered state at finite temperatures. Typically, the realization of 2D magnetism requires the introduction of magnetic anisotropy to break the SO(3) symmetry and open a spin-wave gap, which can be obtained by SOC, crystal fields, and strain.[12,13,52] In contrast, ferroelectricity is exempt from the Mermin–Wagner restriction because it involves the breaking of discrete symmetries and is governed by long-range dipole–dipole interactions.

(2) Depolarization field In the 2D limit, the absence of bulk screening dramatically amplifies the influence of boundary-induced fields. For ferroelectrics, the depolarization field imposes a formidable electrostatic energy penalty that is proportional to $\boldsymbol{P}^2$. Without external charge compensation, this penalty can quench out-of-plane polarization — a challenge far less critical in 3D bulk where carrier screening or domain formation is effective.[53] In contrast, for magnets, the demagnetizing field (dipolar energy) is typically orders of magnitude weaker than the short-range exchange interaction. Consequently, while it dictates shape anisotropy by favoring in-plane alignment, it rarely destabilizes the magnetic order itself, unlike the decisive role played by the depolarization field in ferroelectric phase stability. To circumvent the depolarization field in the 2D limit, three primary strategies have been developed. First, geometric redirection focuses on materials with in-plane polarization, which eliminates surface bound charges and thus avoids the field's penalty entirely.[54] Second, external screening utilizes conductive encapsulation — such as graphene electrodes or ionic adsorbates — to provide charge compensation and neutralize the depolarization field.[15,16] Third, emergent mechanisms, most notably sliding ferroelectricity in vdW bilayers, generate out-of-plane polarization through interlayer lateral shifts.[18,19] This mechanism is intrinsically more robust against traditional depolarization constraints than ion-displacement-based ferroelectricity, enabling stable polar order at the atomic scale.

4. Material realizations of 2D multiferroics

Building upon these theoretical insights and the strategic bypass of physical constraints, the pursuit of 2D multiferroicity has evolved along two primary trajectories. One pathway focuses on the discovery of intrinsic single-phase multiferroics, where magnetic and ferroelectric orders are intertwined within a single crystal lattice through inherent symmetry breaking. The other leverages the versatile vdW platform to create artificially engineered multiferroics, where disparate ferroic orders are coupled across interfaces or induced by interlayer degrees of freedom. In the following sections, we examine representative material systems and experimental milestones that define these two paradigms, highlighting how they navigate the delicate balance between stabilizing long-range order and maintaining functional coupling at the atomic limit.

4.1. Intrinsic 2D multiferroics

Intrinsic 2D multiferroics represent the most conceptually direct realization of multiferroicity, as magnetic and polar orders originate from the same atomic framework. Prominent current examples include: transition metal dihalides represented by NiI_2, transition metal thiophosphates represented by $CuCrP_2S_6$, transition metal dichalcogenides represented by $CuCrX_2$ (which can be regarded as variants of MX_2), transition

metal oxohalides represented by $VOCl_2$, and MXenes represented by $Hf_2VC_2F_2$.

(1) Transition metal dihalides Among the most prominent examples, 2D vdW transition metal dihalides such as NiI_2 have established a clear paradigm for spin-driven multiferroicity in the 2D limit. Experimental evidence from second-harmonic generation (SHG) and linear dichroism (LD) initially identified a multiferroic transition at approximately 21 K in single layers, significantly lower than the bulk value of 60 K (Figs. 3(a) and 3(b)).[55] However, the interpretation of these all-optical signatures has faced scrutiny, with some studies suggesting that these signals might stem from magnetic-order-induced symmetry breaking rather than definitive ferroelectricity.[56]

To address this, recent research has employed scanning tunneling microscopy (STM) to achieve atomic-scale visualization of multiferroic domains, directly observing the periodic modulation of electrostatic potential induced by the spin spiral.[57] Complementing these microscopic insights, transport measurements on few-layer devices have successfully captured ferroelectric hysteresis loops, confirming the coexistence of ferroelectric and antiferroelectric phases[58] (Figs. 3(c)–3(e)).

From a theoretical perspective, the origin of this complex order extends beyond simple exchange frustration. While the competition between near-neighbor ferromagnetic and third-neighbor antiferromagnetic interactions is fundamental,[59] first-principles-based spin Hamiltonian models now emphasize the critical role of the Kitaev interaction in determining the specific in-plane propagation direction and the canting of the rotation plane.[60]

Furthermore, the robust magnetoelectric coupling in NiI_2 is evidenced by the observation of giant chiral magnetoelectric oscillations and electromagnon modes, which represent collective excitations of the entangled magnetic and dipolar orders,[61] as Fig. 3(f) shows. The material's properties remain highly tunable; for instance, hydrostatic pressure has been shown to dramatically increase transition temperatures and induce a reversible transformation from helimagnetic to antiferromagnetic states by modulating interlayer interactions.[62] Additionally, as Figs. 3(g) and 3(h) show, Wang *et al.* discovered orientation-selective spin-polarized edge states using spin-polarized STM in monolayer islands.[63]

Overall, NiI_2 represents a canonical type-II 2D multiferroic system where the intricate competition between frustrated exchange, anisotropic Kitaev interactions, and lattice degrees of freedom manifests in a highly susceptible electronic landscape, capable of hosting sophisticated topological spin textures and coupled collective excitations.

(2) Transition metal thiophosphate Another representative 2D vdW multiferroic material is $CuCrP_2S_6$, which substitutes the In atom in the intrinsic 2D ferroelectric material $CuInP_2S_6$ with a magnetic Cr atom. Early theoretical predictions and experimental efforts established that monolayer and few-layer $CuCrP_2S_6$ host ferromagnetism and electric-field-driven ferroelectricity, with the out-of-plane polarization primarily attributed to the displacement of Cu ions within the sulfur framework,[64] as Fig. 4(a) shows.

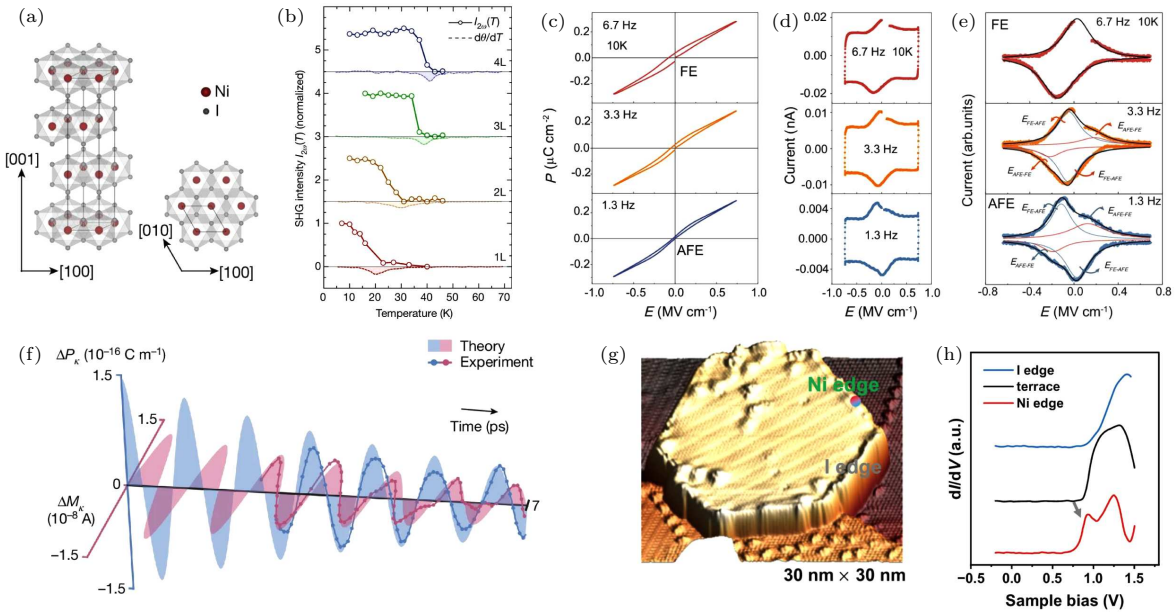


Fig. 3. Experimental results in 2D multiferroic NiI_2. (a) Crystal structure of bulk NiI_2. Reproduced with permission from Ref. [55]. (b) Temperature-dependent SHG measurements of different layer numbers. Reproduced with permission from Ref. [55]. (c)–(e) Frequency-dependent P–E (c) and I–E hysteresis loops (d), (e) of trilayer NiI_2 at 10 K. Reproduced with permission from Ref. [58]. (f) Time-dependent terahertz oscillations of the electric polarization and magnetization extracted from the electromagnon dynamics. Reproduced with permission from Ref. [61]. (g)–(h) Image of the NiI_2 island (g) and the tunneling spectra (h) measured with a magnetic Cr tip display a prominent peak associated with edge states exclusively at the Ni-terminated edge. Reproduced with permission from Ref. [63].

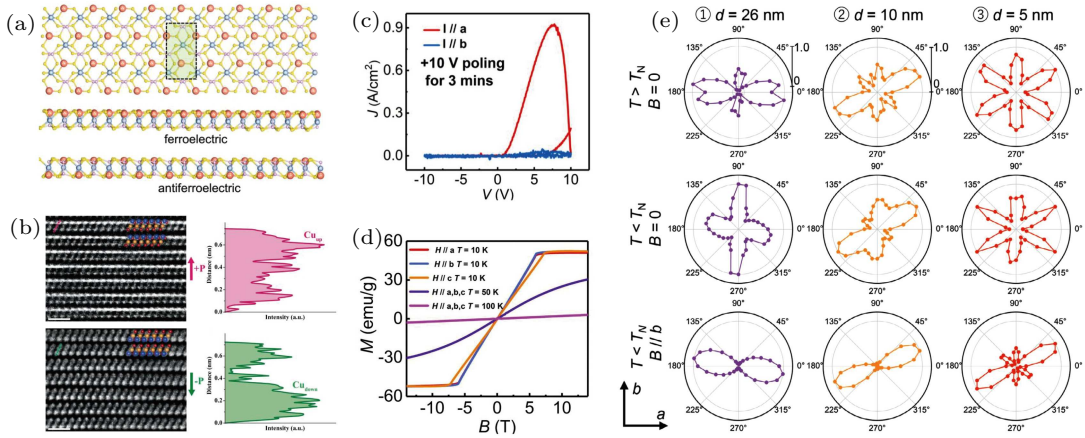


Fig. 4. Experimental results in 2D multiferroic $CuCrP_2S_6$. (a) Top and side views of the ferroelectric and antiferroelectric phases in $CuCrP_2S_6$ monolayer. Reproduced with permission from Ref. [64]. (b) Cross-sectional HAADF-STEM images with corresponding *Z*-contrast intensity profiles. Reproduced with permission from Ref. [66]. (c) The current density versus voltage curves along the *a* and *b* axes. Reproduced with permission from Ref. [67]. (d) Magnetic hysteresis loops measured along different crystallographic orientations. Reproduced with permission from Ref. [67]. (e) Thickness dependence of SHG signals at different temperatures in regions 1 (15 nm thickness), 2 (10 nm thickness), and 3 (5 nm thickness), respectively. Reproduced with permission from Ref. [69].

Subsequent investigations into its magnetic nature revealed an A-type antiferromagnetic ground state with a Néel temperature of 32 K, demonstrating that electric polarization can be modulated by an in-plane magnetic field. This magnetoelectric coupling is fundamentally linked to a spin-direction-dependent p–d hybridization mechanism arising from off-centered Cr^{3+} ions.[65] The structural and physical understanding of $CuCrP_2S_6$ has been further refined through direct atomic-scale observations. As Fig. 4(b) shows, using aberration-corrected scanning transmission electron microscopy, researchers confirmed the presence of intrinsic room-temperature ferroelectricity by identifying the coherent off-center arrangement of Cu atoms.[66]

Parallel studies highlighted significant in-plane electrical and magnetic anisotropies (Figs. 4(c) and 4(d)), identifying the a-axis as the magnetic easy axis and characterizing a spin-flop transition under external fields.[67] Moreover, optimization of crystal growth techniques enabled detailed calorimetric analyses, which pinpointed an antiferroelectric-to-paraelectric transition in the 140–200 K range and elucidated the crystal field splitting behavior of the Cr ions.[68]

Recent advancements have utilized nonlinear optical and vibrational spectroscopy to probe the complex phase diagram of $CuCrP_2S_6$. Optical SHG measurements have successfully tracked structural and magnetic phase transitions, revealing a giant magnetoelectric modulation of SHG signals that is sensitive to the number of atomic layers,[69] as Fig. 4(e) shows. Complementary Raman spectroscopic studies have provided a comprehensive assignment of phonon modes, identifying low-frequency soft modes as distinct fingerprints of the antiferroelectric transition. They also uncovered a significant phonon hardening effect at low temperatures, driven by strong magnetoelastic coupling and negative thermal expansion.[70]

Collectively, these findings establish $CuCrP_2S_6$ as a sophisticated quaternary system where the interplay between copper-ion stochasticity and chromium-ion magnetic order creates a highly tunable landscape of ferroic phase transitions and collective excitations.

(3) Transition metal dichalcogenides The layered dichalcogenide system $ACrX_2$ (A = Cu, Ag; X = S, Se) represents a distinctive class of non-vdW multiferroics characterized by strong magnetoelastic coupling and high-temperature order. Early investigations into bulk $AgCrS_2$ established that an unconventional collinear magnetic structure — consisting of double ferromagnetic stripes coupled antiferromagnetically — triggers a structural transition into a polar monoclinic state via magnetoelastic distortion.[71]

Building upon this bulk physics, first-principles calculations predicted that thinning $CuCrS_2$ and $CuCrSe_2$ to the 2D limit could resolve the intrinsic exclusion between magnetism and ferroelectricity, suggesting that vertical ferroelectricity arises from tetrahedral bonding configurations rather than spin-driven mechanisms.[72] This theoretical outlook was subsequently validated by the synthesis of $CuCrS_2$ nanoflakes exhibiting switchable ferroelectric polarization and an exceptionally high transition temperature of approximately 700 K.[73]

Recent experimental refinements have further uncovered complex layer-dependent and anisotropic properties within this family. In $CuCrSe_2$ nanosheets, remarkable even–odd layer-dependent ferromagnetism was discovered, where even-layer samples exhibit an anomalous Hall effect due to symmetry breaking induced by Cu-orbital shifts,[74] as Fig. 5(a) shows. Direct evidence for multiferroicity in single-layer $CuCrSe_2$ was eventually obtained, confirming the coexistence of room-temperature ferroelectricity and ferromagnetism at 120 K, with the latter driven by a unique ligand-mediated exchange interaction,[75] as Figs. 5(b)–5(e) show. Beyond these fundamental physics, significant progress has been made in the controllable growth of high-temperature ferroelectric $CuCrSe_2$

and the realization of wafer-scale $CuCrS_2$ films for memristive and energy storage applications.[76–78]

Collectively, these findings establish the $ACrX_2$ family as a robust multiferroic platform where the high-energy barrier of cation displacement supports ferroelectric stability, while the magnetic order in the 2D limit is intricately governed by layer-dependent symmetry breaking.

(4) Potential 2D intrinsic multiferroic materials First-principles calculations further suggest that intrinsic 2D multiferroicity may be more widespread than currently realized experimentally. Certain VOX_2 and certain MXenes have been theoretically shown to host coexisting magnetic order and spontaneous polarization stabilized by Jahn–Teller distortions or noncollinear spin textures.

A landmark computational study identified the $Hf_2VC_2F_2$ monolayer as a rare type-II multiferroic, where a noncollinear 120° Y-type spin order directly breaks inversion symmetry to generate ferroelectric polarization,[79] as Figs. 6(a) and 6(b) show. Beyond simple polarization, the coupling between magnetism and lattice in multiferroic MXenes has been shown to stabilize room-temperature magnetic skyrmions, whose topological stability can be electrically manipulated by switching the underlying ferroelectric dipoles.[80]

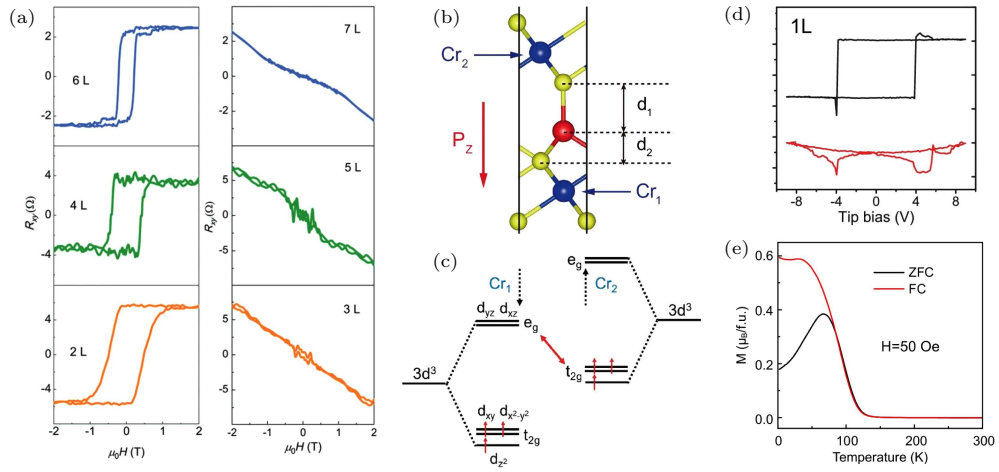


Fig. 5. Experimental results in 2D multiferroic $CuCrX_2$. (a) Layer-dependent magnetic properties in 2D $CuCrSe_2$. Reproduced with permission from Ref. [74]. (b) The atomic structure of single-layer $CuCrSe_2$ exhibits unequal vertical distances between Cu and Se atoms, resulting in a spontaneous out-of-plane electric polarization. Reproduced with permission from Ref. [75]. (c) Vertical polarization induces opposite energy shifts in the e_g and t_{2g} orbitals of the two Cr atoms, reducing the energy gap to stabilize ferromagnetic coupling. Reproduced with permission from Ref. [75]. (d) Off-field PFM measurements on single-layer $CuCrSe_2$, revealing a clear 180° phase hysteresis loop and a butterfly-shaped amplitude curve. Reproduced with permission from Ref. [75]. (e) Temperature-dependent magnetization curves (ZFC and FC) under a 50 Oe field demonstrate a paramagnetic-to-ferromagnetic phase transition. Reproduced with permission from Ref. [75].

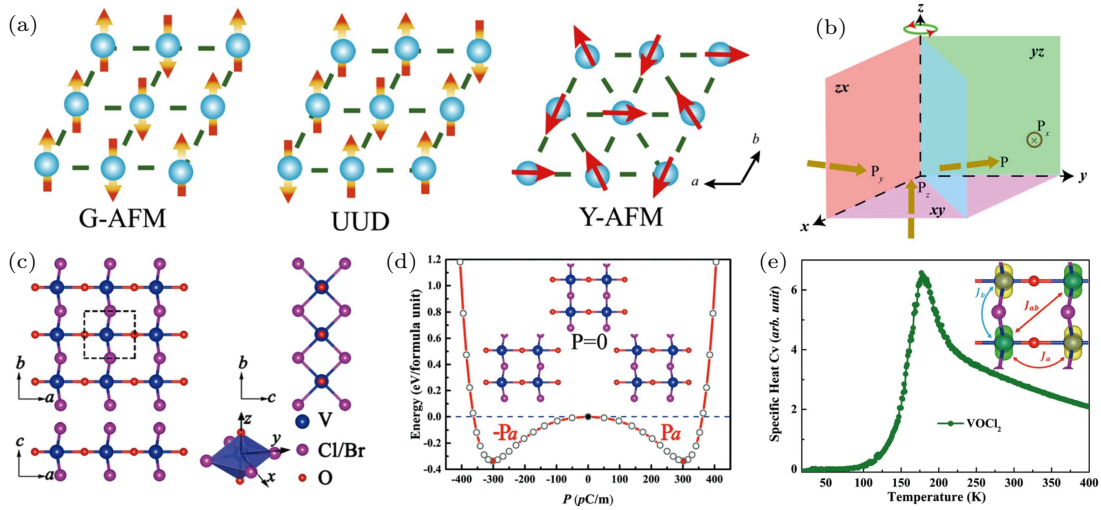


Fig. 6. Calculation results in 2D multiferroic $Hf_2VC_2F_2$ (a), (b) and $VOCl_2$ (c)–(e). (a) Schematics illustrating the competing magnetic configurations on the triangular lattice, including stripe antiferromagnetic (G-AFM), up-up-down ferrimagnetic (UUD), and the noncollinear 120° Y-type antiferromagnetic (Y-AFM) orders. Reproduced with permission from Ref. [79]. (b) A diagram demonstrating the magnetoelectric coupling mechanism, where the ferroelectric polarization vector is generated perpendicular to the spin helical plane and rotates synchronously with it. Reproduced with permission from Ref. [79]. (c) The top and side views of the $VOCl_2$ monolayer reveal the broken inversion symmetry caused by the off-center displacement of V ions. Reproduced with permission from Ref. [81]. (d) The double-well potential energy profile demonstrates the thermodynamic stability of the ferroelectric states and indicates the energy barrier required for polarization reversal. Reproduced with permission from Ref. [81]. (e) The specific heat with respect to temperature. Reproduced with permission from Ref. [81].

In parallel, the transition metal oxyhalide $VOCl_2$ has emerged as a promising candidate, with first-principles evidence suggesting a large intrinsic in-plane polarization driven by pseudo Jahn–Teller distortions alongside stable antiferromagnetism,[81] as the structure, double-well potential energy, and temperature-dependent specific heat are shown in Figs. 6(c)–6(e). This family has been further extended to the altermagnetic regime in VOX_2 (X = Cl, Br, I) monolayers, where the interplay of ferroelectricity and altermagnetism enables a giant bulk spin photovoltaic effect and provides a strategy for nonvolatile multistate memory.[82]

While these theoretical frameworks remain the primary guide, early experimental efforts have begun to report room-temperature ferroelectricity and magnetoelectric coupling in free-standing $Ti_3C_2T_x$ MXene films, attributing the multiferroic behavior to the interaction between disordered dipoles and local spin moments.[83,84] Collectively, these theoretical and early experimental works establish MXenes and oxyhalides as a versatile playground for 2D multiferroicity, where the rich variety of transition metals and functional groups allows for the engineering of high-temperature ferroic orders and complex topological magnetic textures.

4.2. Engineered 2D multiferroics

Beyond intrinsic 2D multiferroics, the coupling of distinct ferroic properties can also be achieved through extrinsic engineering factors such as intercalation, doping, interfaces, or through hetero-composites with interlayer degrees of freedom. By engineering methods, systems with higher critical temperatures can be candidates, while extrinsic factors may introduce new mechanisms to increase the intensity of coupling. In fact, the aforementioned single-phase materials also embody this engineering philosophy. For example, the aforementioned $CuCrSe_2$ can be viewed as intercalating a Cu layer into magnetic $CrSe_2$ layers to form multiferroics.

(1) Doping/intercalation Chemical doping and intercalation offer effective strategies to introduce magnetism into ferroelectric hosts without destroying the noncentrosymmetric lattice. For instance, Yang *et al.* achieved type-I multiferroicity by substituting In sites with Fe ions ($\sim 3.22\%$) in ferroelectric α-In_2Se_3. While the host α-In_2Se_3 is diamagnetic, the Fe-doped $Fe_{0.16}In_{1.84}Se_3$ exhibits ferromagnetism with in-plane anisotropy at 2 K and a Curie temperature of ~ 8 K, as Figs. 7(a) and 7(b) show. PFM and magnetic measurements confirmed the coexistence of ferroelectricity and ferromagnetism, though the magnetoelectric coupling strength remains to be explored.[85] Similarly, Du *et al.* realized room-temperature multiferroicity in SnSe by introducing local $SnSe_2$ microdomains into the ferroelectric SnSe matrix. Unlike intrinsic SnSe, this p-doped system exhibits room-temperature ferrimagnetism (with a Curie temperature approaching ~ 337 K) attributed to enhanced interfacial exchange interactions.[86]

By leveraging an interfacial modulation strategy on c-plane sapphire, researchers synthesized wafer-scale, one-unit-cell non-layered chromium sulfide exhibiting robust multiferroicity. The substrate-induced intralayer sliding of self-intercalated Cr atoms breaks inversion symmetry. Simultaneously, this structural modification enhances superexchange interactions and p–d orbital hybridization, nearly doubling the ferromagnetic Curie temperature to 310 K compared to the bulk and enabling effective electric-field control over magnetic states.[87] Although these engineered systems demonstrate high critical temperatures, the direct coupling between ferroic orders is generally weak.

(2) Sliding ferroelectricity Interlayer sliding ferroelectricity offers a different engineering strategy, exploiting stacking geometry rather than chemistry to generate polarization. In bilayer and moiré systems, relative lateral shifts between layers break inversion symmetry and create switchable dipoles, even when the individual monolayers are centrosymmetric. With interlayer engineering, sliding-induced 2D ferroelectricity has been demonstrated in the topological semimetal WTe_2,[16] metallic twisted bilayer graphene,[88] and insulating AB-stacked bilayer hBN.[19]

When combined with intrinsically magnetic layers such as CrI_3, sliding-induced polarization modifies interlayer exchange and magnetic anisotropy, opening a pathway toward electrically controllable magnetism driven purely by stacking registry. Ji *et al.*[89] generalized bilayer stacking ferroelectricity through layer group analysis, using centrosymmetric CrI_3 to demonstrate how specific stacking configurations break inversion symmetry. Their first-principles calculations identified six symmetry-related energy minima (Fig. 7(c)), characterized by a dominant in-plane component interlocked with a smaller out-of-plane component. This unique coupling enables deterministic out-of-plane switching via in-plane electric fields across remarkably low energy barriers. Crucially, these ferroelectric states coincide with ferromagnetic order — contrasting with the antiferromagnetism of non-polar stackings — thereby establishing a sliding-induced multiferroic state suitable for low-power applications. Although experimental verification of such fully sliding-induced multiferroics remains nascent, these theoretical insights establish a robust framework for exploring functional stacking in 2D magnetic materials.

(3) Heterostructures vdW heterostructures represent a highly versatile platform for engineering 2D multiferroicity. Unlike conventional epitaxial growth, which is limited by lattice matching, vdW assembly allows the vertical stacking of ferromagnetic and ferroelectric layers with atomically sharp interfaces and arbitrary twisting angles. This proximity en-

ables strong magnetoelectric coupling via mechanisms such as charge transfer, strain transfer, or modification of interlayer exchange interactions. The concept was theoretically pioneered by Gong *et al.*, who predicted strong magnetoelectric coupling in the $Cr_2Ge_2Te_6/In_2Se_3$ heterostructure. Their density functional theory (DFT) calculations revealed that reversing the electric polarization of In_2Se_3 switches the magnetocrystalline anisotropy of $Cr_2Ge_2Te_6$ between out-of-plane (easy-axis) and in-plane (easy-plane), effectively toggling the ferromagnetic order,[90] as Fig. 7(d) shows.

Experimentally, Eom *et al.* [91] demonstrated voltage-controlled magnetism in $Fe_{3-x}GeTe_2/In_2Se_3$ devices. Using a magneto-optical Kerr microscope and Raman spectroscopy, they observed a significant modulation of the coercive field in $Fe_{3-x}GeTe_2$ under gate voltages and confirmed that this effect is driven by the piezoelectric tensile strain transferred from the In_2Se_3 layer, which reduces the magnetic anisotropy energy (Figs. 7(e) and 7(f)). More recently, Wu *et al.* [92] achieved nonreciprocal and nonvolatile electric-field switching of magnetism in a CrI_3/α-In_2Se_3 heterostructure. By mapping the magnetic phase transitions via reflective magnetic circular dichroism (Fig. 7(g)), they found that the ferroelectric polarization of In_2Se_3 modulates the interlayer magnetic coupling of CrI_3. Furthermore, theoretical designs have demonstrated that such ferroelectric heterostructures can host purely electrically controllable magnetism even without intrinsic magnetic layers. For instance, in an engineered InSe/In_2Se_3 vdW heterostructure, the switchable out-of-plane polarization of In_2Se_3 can deterministically control the band alignment. When combined with appropriate hole doping, this mechanism enables robust, nonvolatile switching of itinerant ferromagnetism.[93]

These developments highlight the shift from intrinsic multiferroics to rationally designed vdW heterostructures, where the decoupling of lattice-matching constraints allows for unprecedented control over interfacial physics.

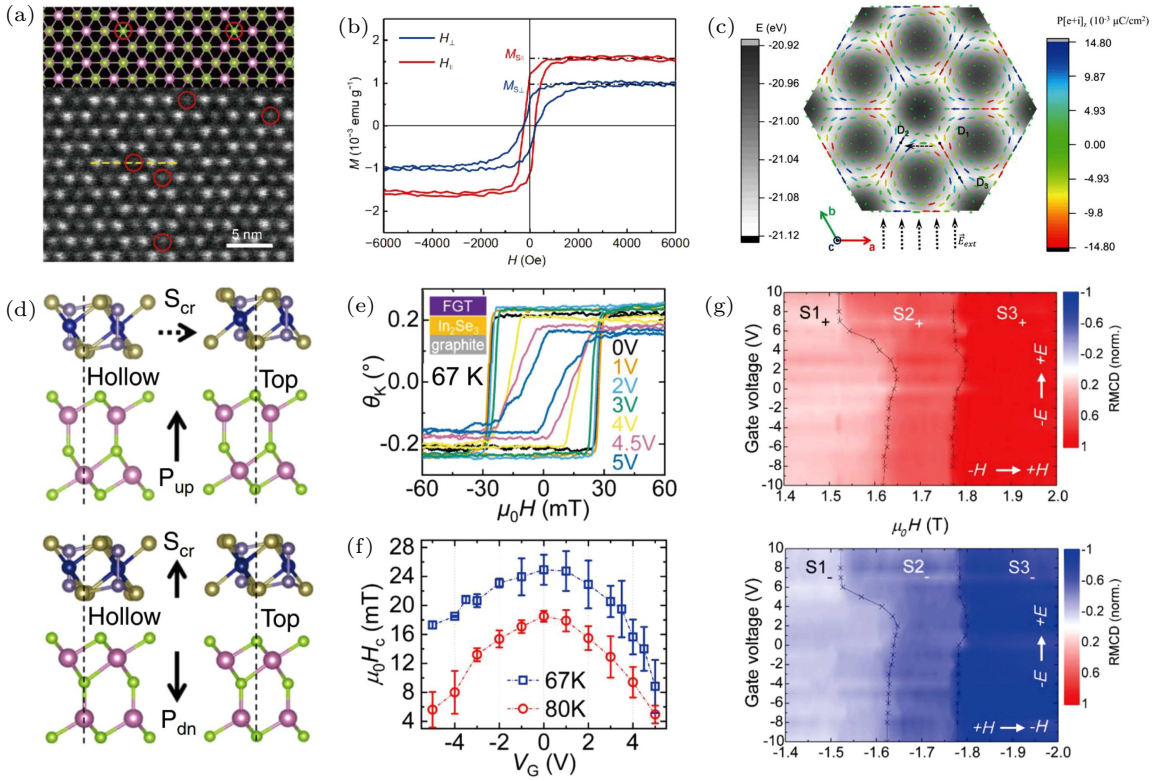


Fig. 7. Strategies for engineered 2D multiferroics: doping (a)–(b), sliding (c), and heterostructures (d)–(g). (a)–(b) High-resolution STEM image (a) and magnetic hysteresis loops (b) of Fe-doped In_2Se_3 confirming homogeneous doping and ferromagnetism with distinct magnetic anisotropy, respectively. Reproduced with permission from Ref. [85]. (c) The calculated potential energy surface for bilayer CrI_3 revealing six degenerate energy minima created by lateral sliding. Reproduced with permission from Ref. [89]. (d) Side views illustrating the switching of the electric polarization of In_2Se_3 modulates the ferromagnetic order on or off. Reproduced with permission from Ref. [90]. (e) Magnetic hysteresis loops of the $Fe_{3-x}GeTe_2/In_2Se_3$ heterostructure measured under positive gate voltages. Reproduced with permission from Ref. [91]. (f) The extracted coercive field plotted against gate voltage, confirming a strain-mediated coupling mechanism driven by the piezoelectric effect. Reproduced with permission from Ref. [91]. (g) Magnetic phase diagrams of the CrI_3/In_2Se_3 heterostructure reveal asymmetric phase boundaries, demonstrating nonreciprocal and nonvolatile modulation of magnetism via ferroelectric switching. Reproduced with permission from Ref. [92].

4.3. Extended topics

While the preceding section provided a comprehensive review of specific 2D multiferroic materials, the potential of 2D systems extends far beyond the static coexistence of magnetism and ferroelectricity. This section explores three pivotal frontiers that are redefining the boundaries of 2D multiferroics: the expansion into novel ferroic degrees of freedom, the functionalization of quasi-one-dimensional domain

walls, and the active manipulation of ferroic orders through non-equilibrium dynamics.

(1) Other ferroic orders Beyond canonical ferromagnetic and ferroelectric orders, the landscape of 2D multiferroics is enriched by emerging ferroic orders such as ferroelasticity,[94–98] ferrotoroidicity,[99–102] and ferroaxiality.[103–108] Integrating these exotic orders with fundamental magnetic or polar states broadens the thermodynamic definition of multiferroicity, offering novel cross-coupling channels beyond traditional magnetoelectric effects.

Among these, 2D ferroelasticity has been experimentally well-established. The multiferroic coupling of magnetism and ferroelasticity is shown in Fig. 8(a). A typical hysteresis behavior obtained experimentally in a β-In_2Se_3 flake is shown in Fig. 8(b). Ferrotoroidicity (Fig. 8(c)) represents a compelling topological order that is actively being explored in 2D antiferromagnetic systems to achieve novel magnetoelectric responses. For ferroaxiality (Fig. 8(d)), robust ferro-rotational (ferroaxial) order and its highly reversible electrical switching have been experimentally demonstrated in nanometer-thick van der Waals 1T-TaS_2 crystals.[109]

Alongside these structural and magnetic topological orders, the ferrovalley order emerges as a uniquely robust and distinct signature inherent to 2D vdW materials. Particularly well defined in hexagonal lattices, this ferroic state manifests as spontaneous valley polarization, where the energetic degeneracy between inequivalent valleys is lifted by the interplay of strong SOC and intrinsic exchange interactions. Defined by the sign of the Berry curvature, this valley degree of freedom is not only theoretically predicted but also readily accessible through circularly polarized light and the anomalous Hall effect, making it a pivotal component of the 2D multiferroic landscape.

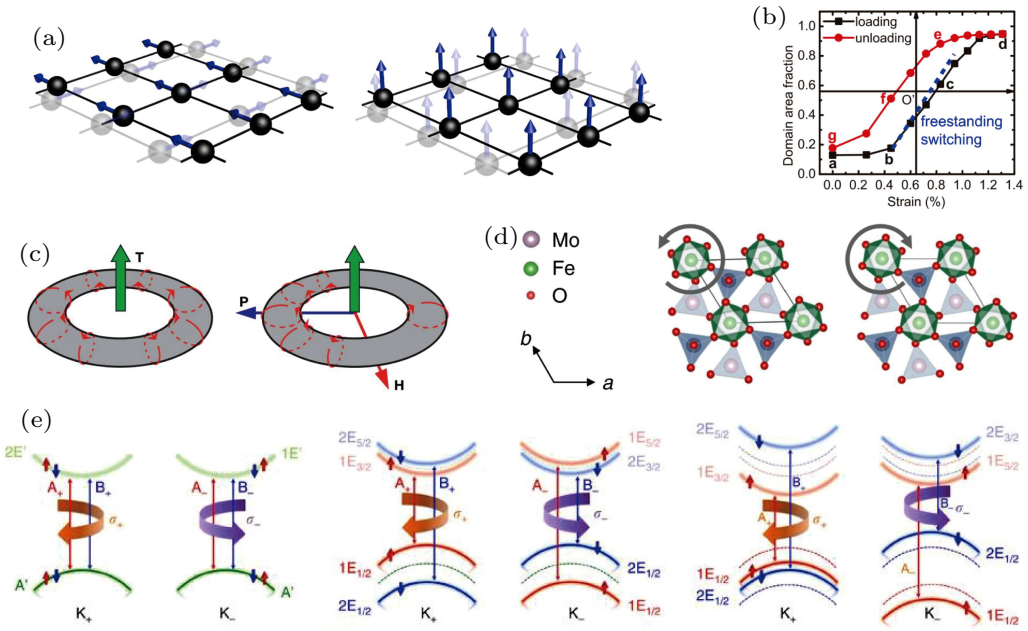


Fig. 8. Other ferroic orders in 2D systems. (a) Schematic illustration of strong multiferroic coupling in 2D tetragonal MX monolayers, where the in-plane magnetic easy axis rotates by 90° accompanying the ferroelastic transition. Reproduced with permission from Ref. [97]. (b) Hysteresis loop under applied uniaxial tensile strain in a vdW β-In_2Se_3 flake. Reproduced with permission from Ref. [98]. (c) Schematic illustration of the toroidal moment originating from a magnetic vortex, and its intrinsic magnetoelectric coupling where an applied magnetic field induces an electric polarization orthogonal to the torus axis. Reproduced with permission from Ref. [99]. (d) Schematic illustration of the ferroaxial order in the multiferroic $RbFe(MoO_4)_2$ lattice, where the coherent counter-rotations of MoO_4 polyhedra break mirror symmetries and generate a macroscopic axial vector order parameter coupled to nonlinear optical fields. Reproduced with permission from Ref. [106]. (e) Conceptual analogy establishing ferrovalley materials where the spontaneous valley polarization (splitting between K and K' valleys) is drawn in parallel to the spontaneous charge polarization in ferroelectrics and spin polarization in ferromagnets. Reproduced with permission from Ref. [113].

Valley polarization was first observed in graphene and 2H-TMDs,[110–112] but the polarization is not spontaneous. Tong *et al.*[113] first predicted ferrovalley in 2H-VSe_2 and developed the concept, as Fig. 8(e) shows. Then ferrovalley was found by calculation in heterostructures of valley materials and magnetic materials, such as $MoTe_2$/EuO and WSe_2/CrI_3.[114,115] Janus monolayer is another possible path.[116,117] Seyler *et al.*[118] experimentally demonstrated the manipulation of valley pseudospins in monolayer WSe_2 via a magnetic proximity effect induced by the 2D ferromagnet CrI_3. Finding materials with coupled ferrovalley and ferroelectricity holds immense promise for next-generation valleytronic devices, particularly for realizing high-density, all-electric memory and logic gates based on the topologically protected anomalous valley Hall effect.

(2) Domain walls Beyond the domains themselves, domain walls (DWs) in 2D multiferroics represent a compelling frontier for exploring lower-dimensional physics. In the ultrathin limit, these boundaries manifest as quasi-one-dimensional topological defects or stacking solitons,[119] serv-

ing as atomically sharp interfaces between degenerate ferroic ground states. Unlike their bulk counterparts, 2D DWs are strictly constrained by the vdW gap and in-plane lattice symmetries, creating unique local environments characterized by substantial strain gradients and localized symmetry breaking.

Consequently, as Figs. 9(a)–9(d) show, the classification of these walls extends beyond the traditional Ising, Néel, and Bloch dichotomy;[120–122] in 2D systems, they are often governed by stacking textures and can be precisely manipulated via moiré engineering. A striking example of unique 2D phenomena is the reversible interconversion between multiferroic domains and domain walls demonstrated by Hassanpour *et al.*,[123] where a three-dimensional multiferroic state is effectively confined into a 2D topological defect, retaining switchable magnetization and polarization, as Fig. 9(e) shows.

Furthermore, these boundaries are not merely static structural features but dynamic entities manipulable at the atomic scale. In monolayer ferroelectrics like In_2Se_3, for instance, scanning tunneling microscopy has revealed that domain boundaries can be driven step-by-step through collective atomic shifting mechanisms (Fig. 9(f)), allowing for deterministic reconfiguration of the domain landscape.[124] Leveraging this mobility, these topologically protected boundaries offer a reconfigurable platform for atomic-scale logic and memory devices, as Fig. 9(g) shows, enabling architectures where the presence or absence of a conductive wall defines the logic state for non-volatile resistive switching.[125]

The physical basis for such applications lies in the reduction of dimensionality, which transforms DWs into functional 1D channels. Owing to their distinct local symmetry and nontrivial topology, they host emergent phenomena absent in the parent domains, such as the emergence of metallic conductivity in nominally insulating ferroelectrics. Seidel *et al.*[126] observed room-temperature electronic conductivity at ferroelectric domain walls in the insulating multiferroic $BiFeO_3$; the piezoresponse force microscopy and conductive atomic force microscopy maps are shown in Figs. 9(h) and 9(i). This conductivity is often strictly confined to specific wall orientations or charge states (head-to-head/tail-to-tail configurations), effectively creating reconfigurable conductive nanowires. Although $BiFeO_3$ is a canonical three-dimensional bulk multiferroic rather than a 2D material, it serves as a powerful conceptual prototype here. It is highly anticipated that analogous phenomena — where domain walls act as reconfigurable 1D conducting channels — are being actively pursued and will be realized in emerging 2D multiferroic systems. In conclusion, DWs can be viewed not only as the interface of multiferroic domains, but also as separate devices with unique functions.

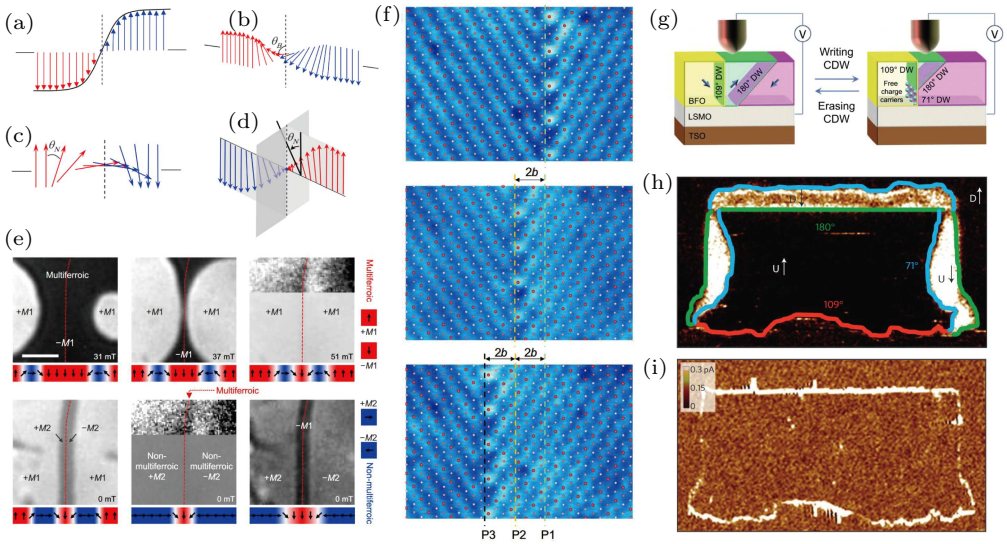


Fig. 9. Research on domain walls. (a)–(d) Schematic illustrations contrasting traditional Ising (a), Bloch (b), Néel (c), and mixed Ising–Néel (d) domain walls. Reproduced with permission from Ref. [120]. (e) Faraday rotation microscopy images visualizing the reversible transformation process where a bulk multiferroic domain is spatially confined into a domain wall and subsequently expanded back into a domain under controlled fields. Reproduced with permission from Ref. [123]. (f) Sequential scanning tunneling microscopy images demonstrating the deterministic, step-by-step manipulation of a 60° tail-to-tail domain boundary in monolayer ferroelectric In_2Se_3 driven by a tip-induced electric field. Reproduced with permission from Ref. [124]. (g) A prototype resistive switching device based on $BiFeO_3$ thin films, illustrating the reversible creation and erasure of highly conductive charged domain walls. Reproduced with permission from Ref. [125]. (h)–(i) Correlated piezoresponse force microscopy (h) and conductive atomic force microscopy maps (i) revealing that room-temperature electronic conductivity in $BiFeO_3$ is selectively confined to 109° and 180° domain walls, while 71° walls remain insulating. Reproduced with permission from Ref. [126].

(3) Non-equilibrium effects Beyond static coupling, non-equilibrium dynamics offer a route to ultrafast functionality by enabling the manipulation of order parameters on picosecond to femtosecond timescales — orders of magnitude faster than conventional switching. Using time-resolved x-ray scattering, Daranciang *et al.*[127] observed a two-step process: an initial lattice contraction caused by shift currents, followed by a long-lived expansion as photogenerated carriers screen the internal depolarization field, as Figs. 10(a) and 10(b) show. Mankowsky *et al.*[128] demonstrated ultrafast reversal of ferro-

electric polarization in $LiNbO_3$ by resonantly exciting a high-frequency phonon mode. The bidirectional switching on a sub-picosecond time scale is shown in Fig. 10(c). In the 2D vdW ferroelectric $NbOI_2$, time-resolved measurements reveal an initial polarization suppression due to photo-carrier screening, followed by a transient enhancement lasting over 200 ps. This prolonged state is sustained by laser-induced coherent acoustic phonons and piezoelectric coupling.[129] The uniform displacement of diffraction spots along the polar axis and the corresponding time-resolved electron beam deflection are shown in Figs. 10(d) and 10(e).

Optical and THz pulses can be used not only to probe but also to actively modulate ferroic properties, such as inducing phase transitions or generating coherent acoustic phonons. By driving materials into non-equilibrium regimes, researchers can access transient states inaccessible via thermodynamic pathways, unlocking novel functional behaviors. For instance, Morimoto *et al.*[130] demonstrated that intense terahertz pulses can induce a large macroscopic polarization in paraelectric TTF-CA (Fig. 10(f)). Li *et al.*[131] demonstrated optically induced polarization switching in ferroelectric heterostructures composed of $BaTiO_3$ and MoS_2 (Fig. 10(g)). Luo *et al.*[132] employed megaelectronvolt ultrafast electron diffraction to resolve the ultrafast, anisotropic in-plane strain in layered GeS. Upon photoexcitation, GeS undergoes significant structural deformation, as Figs. 10(h) and 10(i) show. Crucially, this response bypasses conventional thermal expansion; instead, it is governed by a synergy of deformation potentials from electronic redistribution and converse piezoelectric effects triggered by photoinduced transient electric fields.

Collectively, these works demonstrate that driving ferroelectric and multiferroic materials into non-equilibrium regimes via optical or terahertz stimuli allows for the deterministic manipulation of lattice strain and polarization on femtosecond-to-picosecond timescales, bypassing thermodynamic constraints to unlock ultrafast functional behaviors.

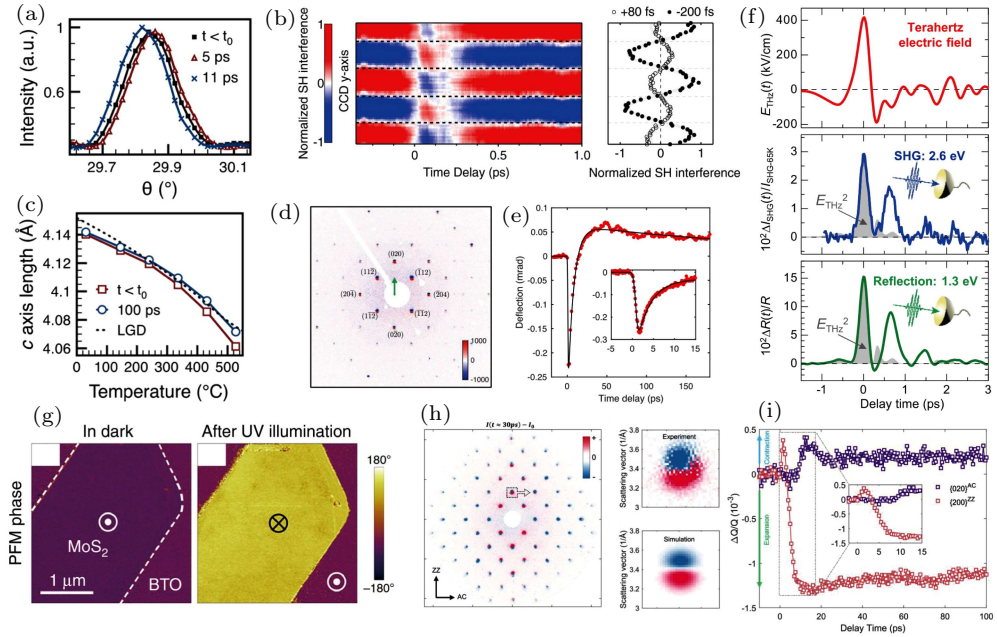


Fig. 10. Non-equilibrium effects related to ferroic properties. (a)–(b) Time-resolved x-ray diffraction scans (a) revealing ultrafast lattice dynamics and the comparison of the observed lattice expansion with Landau–Ginzburg–Devonshire theory (b) in $PbTiO_3$. Reproduced with permission from Ref. [127]. (c) Time-resolved second-harmonic interference fringes exhibit a transient 180° phase shift, directly confirming the sign inversion of the nonlinear susceptibility and the ultrafast reversal of the ferroelectric polarization in $LiNbO_3$. Reproduced with permission from Ref. [128]. (d)–(e) The uniform displacement of diffraction spots along the polar axis (d) and the corresponding time-resolved electron beam deflection (e) reveal an initial suppression followed by a transient enhancement of the ferroelectric polarization in $NbOI_2$. Reproduced with permission from Ref. [129]. (f) The temporal profiles of the driving terahertz electric field, induced second-harmonic generation, and reflectivity change demonstrate that the ultrafast macroscopic polarization and charge transfer modulation in the paraelectric phase are coherently driven by the instantaneous electric field intensity in TTF-CA. Reproduced with permission from Ref. [130]. (g) PFM phase images of the $MoS_2/BaTiO_3$ heterostructure acquired in the dark and after UV illumination, demonstrating optically induced polarization reversal in the region covered by the MoS_2 flake. Reproduced with permission from Ref. [131]. (h)–(i) Differential diffraction patterns (h) and time-resolved lattice dynamics (i) of layered GeS demonstrating a highly anisotropic ultrafast optomechanical response, characterized by a simultaneous expansion along the zigzag direction and contraction along the armchair direction on a 10 ps timescale. Reproduced with permission from Ref. [132].

In summary, the evolution of 2D multiferroics is characterized by a transition from the study of static, macroscopic domains to the mastery of complex, multi-dimensional degrees of freedom. The emergence of exotic orders such as ferrovalley and ferroaxiality broadens the thermodynamic boundaries of multiferroicity, providing novel cross-coupling channels beyond traditional spin-driven magnetoelectric effects. Meanwhile, the confinement of these orders within quasi-1D domain walls introduces a localized, reconfigurable functional landscape. When these spatial textures are coupled with ultrafast, non-equilibrium excitations, a new paradigm of materials control emerges — one where ferroic states can be manipu-

lated at the atomic scale and on femtosecond timescales, effectively bypassing static thermodynamic energy barriers. The synergy between these emerging ferroic orders, topological boundaries, and transient dynamics not only challenges our fundamental understanding of condensed matter physics but also lays the foundation for a new generation of multifunctional quantum devices that are simultaneously faster, smaller, and more energy-efficient than current semiconductor technologies.

5. Summary and outlook

Multiferroicity links distinct order parameters and enables cross-control between their conjugate fields. Extensive studies of bulk multiferroics have established a solid microscopic framework and revealed diverse coupling mechanisms, yet they have also exposed a persistent limitation: materials with robust ferroelectric polarization and high transition temperatures typically exhibit weak magnetoelectric coupling, whereas systems with strong coupling often rely on magnetically driven mechanisms that yield small polarization and low critical temperatures. This long-standing trade-off between the robustness of individual ferroic orders and the strength of their coupling has fundamentally constrained both the physical understanding and technological deployment of multiferroics.

The emergence of 2D materials provides a qualitatively new setting in which this dilemma can be revisited. Reduced dimensionality reshapes symmetry constraints, amplifies the role of SOC, and elevates interfaces, stacking geometry, and interlayer registry to active control parameters. Recent demonstrations of stable 2D ferromagnetism and ferroelectricity show that ferroic orders can persist in the atomic limit when anisotropy, confinement, and lattice degrees of freedom are properly engineered. 2D platforms enable coupling mechanisms without direct bulk analogues, including interlayer sliding, moiré reconstruction, proximity-induced anisotropy, and interfacial charge redistribution, offering an expanded design space in which polarization and magnetism can interact more flexibly.

The roadmap toward high-performance 2D multiferroics, however, is contingent upon overcoming the scarcity of systems that operate reliably at room temperature. Recently, a significant milestone has been achieved with the demonstration of intrinsic room-temperature multiferroicity and voltage-controllable magnetic order in air-stable bilayer $CrTe_2$.[133] Quantitative characterization of magnetoelectric coupling in atomically thin systems is experimentally demanding, and disentangling intrinsic effects from substrate, strain, or electrostatic influences requires further methodological advances. Looking ahead, progress will rely on the continued integration of first-principles theory, symmetry analysis, advanced synthesis, and high-resolution characterization. Beyond equilibrium phases, domain-wall functionalities and nonequilibrium dynamics provide additional avenues for enhancing or redefining magnetoelectric behavior. Together, these efforts position 2D multiferroics not merely as reduced-dimensional extensions of bulk materials, but as a distinct platform for exploring magnetoelectric coupling and for advancing future information technologies.

References

[1] Spaldin N A and Ramesh R 2019 *Nat. Mater.* **18** 203
[2] Fiebig M, Lottermoser T, Meier D and Trassin M 2016 *Nat. Rev. Mater.* **1** 16046
[3] Wang J, Neaton J B, Zheng H, Nagarajan V, Ogale S B, Liu B, Viehland D, Vaithyanathan V, Schlom D G, Waghmare U V, Spaldin N A, Rabe K M, Wuttig M and Ramesh R 2003 *Science* **299** 1719
[4] Zhao T, Scholl A, Zavaliche F, Lee K, Barry M, Doran A, Cruz M P, Chu Y H, Ederer C, Spaldin N A, Das R R, Kim D M, Baek S H, Eom C B and Ramesh R 2006 *Nat. Mater.* **5** 823
[5] Catalan G and Scott J F 2009 *Adv. Mater.* **21** 2463
[6] Kimura T, Goto T, Shintani H, Ishizaka K, Arima T and Tokura Y 2003 *Nature* **426** 55
[7] Goto T, Kimura T, Lawes G, Ramirez A P and Tokura Y 2004 *Phys. Rev. Lett.* **92** 257201
[8] Van Aken B B, Palstra T T M, Filippetti A and Spaldin N A 2004 *Nat. Mater.* **3** 164
[9] Hill N A 2000 *J. Phys. Chem. B* **104** 6694
[10] Novoselov K S, Geim A K, Morozov S V, Jiang D, Zhang Y, Dubonos S V, Grigorieva I V and Firsov A A 2004 *Science* **306** 666
[11] Geim A K and Grigorieva I V 2013 *Nature* **499** 419
[12] Huang B, Clark G, Navarro-Moratalla E, Klein D R, Cheng R, Seyler K L, Zhong D, Schmidgall E, McGuire M A, Cobden D H, Yao W, Xiao D, Jarillo-Herrero P and Xu X 2017 *Nature* **546** 270
[13] Gong C, Li L, Li Z, Ji H, Stern A, Xia Y, Cao T, Bao W, Wang C, Wang Y, Qiu Z Q, Cava R J, Louie S G, Xia J and Zhang X 2017 *Nature* **546** 265
[14] Bai L, Ke C, Luo Z, Zhu T, You L and Liu S 2024 *ACS Nano* **18** 26103
[15] Liu F, You L, Seyler K L, Li X, Yu P, Lin J, Wang X, Zhou J, Wang H, He H, Pantelides S T, Zhou W, Sharma P, Xu X, Ajayan P M, Wang J and Liu Z 2016 *Nat. Commun.* **7** 12357
[16] Fei Z, Zhao W, Palomaki T A, Sun B, Miller M K, Zhao Z, Yan J, Xu X and Cobden D H 2018 *Nature* **560** 336
[17] Sharma P, Xiang F X, Shao D F, Zhang D, Tsymbal E Y, Hamilton A R and Seidel J 2019 *Sci. Adv.* **5** eaax5080
[18] Vizner Stern M, Waschitz Y, Cao W, Nevo I, Watanabe K, Taniguchi T, Sela E, Urbakh M, Hod O and Ben Shalom M 2021 *Science* **372** 1462
[19] Yasuda K, Wang X, Watanabe K, Taniguchi T and Jarillo-Herrero P 2021 *Science* **372** 1458
[20] Tang X and Kou L 2019 *J. Phys. Chem. Lett.* **10** 6634
[21] Gao Y, Gao M and Lu Y 2021 *Nanoscale* **13** 19324
[22] Landau L D 1937 *Zh. Eksp. Teor. Fiz* **7** 926
[23] Kibble T W B 1976 *J. Phys. A: Math. Gen.* **9** 1387
[24] Aizu K 1970 *Phys. Rev. B* **2** 754
[25] Newnham R E and Cross L E 1974 *Mater. Res. Bull.* **9** 927
[26] Newnham R E and Cross L E 1974 *Mater. Res. Bull.* **9** 1021
[27] Schmid H 1994 *Ferroelectrics* **162** 317
[28] Khomskii D 2009 *Physics* **2** 20
[29] Eerenstein W, Mathur N D and Scott J F 2006 *Nature* **442** 759
[30] Mostovoy M 2006 *Phys. Rev. Lett.* **96** 067601
[31] Dong S, Xiang H and Dagotto E 2019 *Natl. Sci. Rev.* **6** 629
[32] Szilva A, Kvashnin Y, Stepanov E A, Nordström L, Eriksson O, Lichtenstein A I and Katsnelson M I 2023 *Rev. Mod. Phys.* **95** 035004
[33] Anderson P W 1959 *Phys. Rev.* **115** 2
[34] Dzyaloshinsky I 1958 *J. Phys. Chem. Solids* **4** 241
[35] Moriya T 1960 *Phys. Rev.* **120** 91
[36] King-Smith R D and Vanderbilt D 1993 *Phys. Rev. B* **47** 1651
[37] Dawber M, Rabe K M and Scott J F 2005 *Rev. Mod. Phys.* **77** 1083
[38] Wang C, You L, Cobden D and Wang J 2023 *Nat. Mater.* **22** 542
[39] Seshadri R and Hill N A 2001 *Chem. Mater.* **13** 2892
[40] Cohen R E 1992 *Nature* **358** 136

[41] Ikeda N, Ohsumi H, Ohwada K, Ishii K, Inami T, Kakurai K, Murakami Y, Yoshii K, Mori S, Horibe Y and Kitô H 2005 *Nature* **436** 1136
[42] Tokura Y, Seki S and Nagaosa N 2014 *Rep. Prog. Phys.* **77** 076501
[43] Zhou Y, Wang Z, Wang F, Ye H and Dong S 2026 *Chin. Phys. B* **35** 027501
[44] Katsura H, Nagaosa N and Balatsky A V 2005 *Phys. Rev. Lett.* **95** 057205
[45] Arima T 2007 *J. Phys. Soc. Jpn.* **76** 073702
[46] Lee N, Choi Y J, Ramazanoglu M, Ratcliff W, Kiryukhin V and Cheong S W 2011 *Phys. Rev. B* **84** 020101
[47] Cao Y, Fatemi V, Fang S, Watanabe K, Taniguchi T, Kaxiras E and Jarillo-Herrero P 2018 *Nature* **556** 43
[48] Cao Y, Fatemi V, Demir A, Fang S, Tomarken S L, Luo J Y, Sanchez-Yamagishi J D, Watanabe K, Taniguchi T, Kaxiras E, Ashoori R C and Jarillo-Herrero P 2018 *Nature* **556** 80
[49] Bistritzer R and MacDonald A H 2011 *Proc. Natl. Acad. Sci. USA* **108** 12233
[50] Mermin N D and Wagner H 1966 *Phys. Rev. Lett.* **17** 1133
[51] Hohenberg P C 1967 *Phys. Rev.* **158** 383
[52] Burch K S, Mandrus D and Park J G 2018 *Nature* **563** 47
[53] Junquera J and Ghosez P 2003 *Nature* **422** 506
[54] Chang K, Liu J, Lin H, Wang N, Zhao K, Zhang A, Jin F, Zhong Y, Hu X, Duan W, Zhang Q, Fu L, Xue Q K, Chen X and Ji S H 2016 *Science* **353** 274
[55] Song Q, Occhialini C A, Ergeçen E, Ilyas B, Amoroso D, Barone P, Kapeghian J, Watanabe K, Taniguchi T, Botana A S, Picozzi S, Gedik N and Comin R 2022 *Nature* **602** 601
[56] Jiang Y, Wu Y, Zhang J, Wei J, Peng B and Qiu C W 2023 *Nature* **619** E40
[57] Amini M, Fumega A O, González-Herrero H, Vaňo V, Kezilebieke S, Lado J L and Liljeroth P 2024 *Adv. Mater.* **36** 2311342
[58] Wu Y, Zeng Z, Lu H, Han X, Yang C, Liu N, Zhao X, Qiao L, Ji W, Che R, Deng L, Yan P and Peng B 2024 *Nat. Commun.* **15** 8616
[59] Fumega A O and Lado J L 2022 *2D Mater.* **9** 025010
[60] Li X, Xu C, Liu B, Li X, Bellaiche L and Xiang H 2023 *Phys. Rev. Lett.* **131** 036701
[61] Gao F Y, Peng X, Cheng X, Viñas Boström E, Kim D S, Jain R K, Vishnu D, Raju K, Sankar R, Lee S F, Sentef M A, Kurumaji T, Li X, Tang P, Rubio A and Baldini E 2024 *Nature* **632** 273
[62] Liu Q, Su W, Gu Y, Zhang X, Xia X, Wang L, Xiao K, Zhang N, Cui X, Huang M, Wei C, Zou X, Xi B, Mei J W and Dai J F 2025 *Nat. Commun.* **16** 4221
[63] Wang Y, Zhao X, Yao L, Liu H, Cheng P, Zhang Y, Feng B, Ma F, Zhao J, Sun J, Wu K and Chen L 2024 *Nat. Commun.* **15** 10916
[64] Lai Y, Song Z, Wan Y, Xue M, Wang C, Ye Y, Dai L, Zhang Z, Yang W, Du H and Yang J 2019 *Nanoscale* **11** 5163
[65] Park C B, Shahee A, Kim K, Patil D R, Guda S A, Ter-Oganessian N and Kim K H 2022 *Adv. Electron. Mater.* **8** 2101072
[66] Io W F, Pang S Y, Wong L W, Zhao Y, Ding R, Mao J, Zhao Y, Guo F, Yuan S, Zhao J, Yi J and Hao J 2023 *Nat. Commun.* **14** 7304
[67] Wang X, Shang Z, Zhang C, *et al.* 2023 *Nat. Commun.* **14** 840
[68] Selter S, Bestha K K, Bhattacharyya P, Özer B, Shemerliuk Y, Roslova M, Vinokurova E, Corredor L T, Veyrat L, Wolter A U B, Hozoi L, Büchner B and Aswartham S 2023 *Phys. Rev. Mater.* **7** 033402
[69] Aoki S, Dong Y, Wang Z, Huang X S W, Itahashi Y M, Ogawa N, Ideue T and Iwasa Y 2024 *Adv. Mater.* **36** 2312781
[70] Tang J, Lawrie B J, Cheng M, Wu Y C, Zhao H, Kong D, Lu R, Yao C H, Gai Z, Li A P, Li M and Ling X 2025 *J. Phys. Chem. Lett.* **16** 4336
[71] Damay F, Martin C, Hardy V, André G, Petit S and Maignan A 2011 *Phys. Rev. B* **83** 184413
[72] Zhong T, Li X, Wu M and Liu J M 2020 *Natl. Sci. Rev.* **7** 373
[73] Xu X, Zhong T, Zuo N, Li Z, Li D, Pi L, Chen P, Wu M, Zhai T and Zhou X 2022 *ACS Nano* **16** 8141
[74] Peng J, Su Y, Lv H, Wu J, Liu Y, Wang M, Zhao J, Guo Y, Wu X, Wu C and Xie Y 2023 *Adv. Mater.* **35** 2209365
[75] Sun Z, Su Y, Zhi A, Gao Z, Han X, Wu K, Bao L, Huang Y, Shi Y, Bai X, Cheng P, Chen L, Wu K, Tian X, Wu C and Feng B 2024 *Nat. Commun.* **15** 4252
[76] Wang P, Zhao Y, Na R, *et al.* 2024 *Adv. Mater.* **36** 2400655
[77] Yu K, Wang H, Liu W, Fu Z, Feng Y, Tang W, Han L, Nie Y, Li D, Zhou Z, Li J, Pan A and Gao L 2025 *Sci. China Mater.* **68** 2868
[78] Fayaz M, Muzaffar M U, Idrees M and Lin Z 2025 *ACS Appl. Nano Mater.* **8** 16299
[79] Zhang J J, Lin L, Zhang Y, Wu M, Yakobson B I and Dong S 2018 *J. Am. Chem. Soc.* **140** 9768
[80] Wang L, Ga Y, Li P, Yu D, Jiang J, Liang J, Wang S and Yang H 2023 *Phys. Rev. B* **108** 054440
[81] Ai H, Song X, Qi S, Li W and Zhao M 2019 *Nanoscale* **11** 1103
[82] Yang Y 2025 *Phys. Rev. B* **112** 104427
[83] Tahir R, Zahra S A, Naeem U, Akinwande D and Rizwan S 2022 *RSC Adv.* **12** 24571
[84] Tahir R, Fatima S, Zahra S A, Akinwande D, Li H, Jafri S H M and Rizwan S 2023 *npj 2D Mater. Appl.* **7** 7
[85] Yang H, Pan L, Xiao M, Fang J, Cui Y and Wei Z 2020 *Sci. China Mater.* **63** 421
[86] Du R, Wang Y, Cheng M, Wang P, Li H, Feng W, Song L, Shi J and He J 2022 *Nat. Commun.* **13** 6130
[87] Song L, Zhao Y, Xu B, *et al.* 2024 *Nat. Commun.* **15** 721
[88] Zheng Z, Ma Q, Bi Z, De La Barrera S, Liu M H, Mao N, Zhang Y, Kiper N, Watanabe K, Taniguchi T, Kong J, Tisdale W A, Ashoori R, Gedik N, Fu L, Xu S Y and Jarillo-Herrero P 2020 *Nature* **588** 71
[89] Ji J, Yu G, Xu C and Xiang H J 2023 *Phys. Rev. Lett.* **130** 146801
[90] Gong C, Kim E M, Wang Y, Lee G and Zhang X 2019 *Nat. Commun.* **10** 2657
[91] Eom J, Lee I H, Kee J Y, *et al.* 2023 *Nat. Commun.* **14** 5605
[92] Wu Y, Zhang D, Zhang Y N, Deng L and Peng B 2024 *Nano Lett.* **24** 5929
[93] Jiang X, Wang Z, Li C, Sun X, Yang L, Li D, Cui B and Liu D 2024 *Chin. Phys. Lett.* **41** 057501
[94] Li W and Li J 2016 *Nat. Commun.* **7** 10843
[95] Wang H and Qian X 2017 *2D Mater.* **4** 015042
[96] Zhang C, Nie Y, Sanvito S and Du A 2019 *Nano Lett.* **19** 1366
[97] Xuan X, Guo W and Zhang Z 2022 *Phys. Rev. Lett.* **129** 047602
[98] Xu C, Mao J, Guo X, Yan S, Chen Y, Lo T W, Chen C, Lei D, Luo X, Hao J, Zheng C and Zhu Y 2021 *Nat. Commun.* **12** 3665
[99] Van Aken B B, Rivera J P, Schmid H and Fiebig M 2007 *Nature* **449** 702
[100] Ederer C and Spaldin N A 2007 *Phys. Rev. B* **76** 214404
[101] Spaldin N A, Fiebig M and Mostovoy M 2008 *J. Phys.: Condens. Matter* **20** 434203
[102] Hayashida T, Misawa R, Fiebig M and Kimura T 2024 *Phys. Rev. B* **109** L100401
[103] Gopalan V and Litvin D B 2011 *Nat. Mater.* **10** 376
[104] Cheong S W, Talbayev D, Kiryukhin V and Saxena A 2018 *npj Quantum Mater.* **3** 19
[105] Hayashida T, Uemura Y, Kimura K, Matsuoka S, Morikawa D, Hirose S, Tsuda K, Hasegawa T and Kimura T 2020 *Nat. Commun.* **11** 4582
[106] Jin W, Drueke E, Li S, Admasu A, Owen R, Day M, Sun K, Cheong S W and Zhao L 2020 *Nat. Phys.* **16** 42
[107] Hayashida T, Uemura Y, Kimura K, Matsuoka S, Hagihala M, Hirose S, Morioka H, Hasegawa T and Kimura T 2021 *Phys. Rev. Mater.* **5** 124409
[108] He Z and Khalsa G 2024 *Phys. Rev. Res.* **6** 043220
[109] Liu G, Qiu T, He K, Liu Y, Lin D, Ma Z, Huang Z, Tang W, Xu J, Watanabe K, Taniguchi T, Gao L, Wen J, Liu J M, Yan B and Xi X 2023 *Nat. Nanotechnol.* **18** 854
[110] Rycerz A, Tworzydło J and Beenakker C W J 2007 *Nat. Phys.* **3** 172
[111] Garcia-Pomar J L, Cortijo A and Nieto-Vesperinas M 2008 *Phys. Rev. Lett.* **100** 236801
[112] Zeng H, Dai J, Yao W, Xiao D and Cui X 2012 *Nat. Nanotechnol.* **7** 490
[113] Tong W Y, Gong S J, Wan X and Duan C G 2016 *Nat. Commun.* **7** 13612
[114] Zhang Q, Yang S A, Mi W, Cheng Y and Schwingenschlögl U 2016 *Adv. Mater.* **28** 959
[115] Xie J, Jia L, Shi H, Yang D and Si M 2019 *Jpn. J. Appl. Phys.* **58** 010906
[116] Lu A Y, Zhu H, Xiao J, Chuu C P, Han Y, Chiu M H, Cheng C C, Yang C W, Wei K H, Yang Y, Wang Y, Sokaras D, Nordlund D, Yang P, Muller D A, Chou M Y, Zhang X and Li L J 2017 *Nat. Nanotechnol.* **12** 744
[117] Feng Y, Qi S, Ren Y, Liu M, Liu N, Liu M, Yang Q and Meng S 2025 *npj Comput. Mater.* **11** 264

[118] Seyler K L, Zhong D, Huang B, Linpeng X, Wilson N P, Taniguchi T, Watanabe K, Yao W, Xiao D, McGuire M A, Fu K M C and Xu X 2018 *Nano Lett.* **18** 3823
[119] Vaezi A, Liang Y, Ngai D H, Yang L and Kim E A 2013 *Phys. Rev. X* **3** 021018
[120] Lee D, Behera R K, Wu P, Xu H, Li Y L, Sinnott S B, Phillpot S R, Chen L Q and Gopalan V 2009 *Phys. Rev. B* **80** 060102
[121] Catalan G, Seidel J, Ramesh R and Scott J F 2012 *Rev. Mod. Phys.* **84** 119
[122] Evans D M, Garcia V, Meier D and Bibes M 2020 *Phys. Sci. Rev.* **5** 20190067
[123] Hassanpour E, Weber M C, Zemp Y, Kuerten L, Bortis A, Tokunaga Y, Taguchi Y, Tokura Y, Cano A, Lottermoser Th and Fiebig M 2021 *Nat. Commun.* **12** 2755
[124] Zhang F, Wang Z, Liu L, Nie A, Li Y, Gong Y, Zhu W and Tao C 2024 *Nat. Commun.* **15** 718
[125] Bednyakov P S, Sturman B I, Sluka T, Tagantsev A K and Yudin P V 2018 *npj Comput. Mater.* **4** 65
[126] Seidel J, Martin L W, He Q, *et al.* 2009 *Nat. Mater.* **8** 229
[127] Daranciang D, Highland M J, Wen H, *et al.* 2012 *Phys. Rev. Lett.* **108** 087601
[128] Mankowsky R, Von Hoegen A, Först M and Cavalleri A 2017 *Phys. Rev. Lett.* **118** 197601
[129] Wang Y, Hossain M S, Li T, Xiong Y, Le C, Kuebler J, Raghavan N, Fernandez-Ballester L, Hong X, Sinitskii A and Centurion M 2025 *Nat. Commun.* **16** 8132
[130] Morimoto T, Miyamoto T, Yamakawa H, Terashige T, Ono T, Kida N and Okamoto H 2017 *Phys. Rev. Lett.* **118** 107602
[131] Li T, Lipatov A, Lu H, Lee H, Lee J W, Torun E, Wirtz L, Eom C B, Íñiguez J, Sinitskii A and Gruverman A 2018 *Nat. Commun.* **9** 3344
[132] Luo D, Zhang B, Sie E J, Nyby C M, Fan Q, Shen X, Reid A H, Hoffmann M C, Weathersby S, Wen J, Qian X, Wang X and Lindenberg A M 2023 *Nano Lett.* **23** 2287
[133] Tian D, Zhong S, Dong J, *et al.* 2026 *Nat. Mater.* **25** 956